# Imaging Integrin $\alpha_v\beta_3$ on Blood Vessels with $^{111}$In-RGD$_2$ in Head and Neck Tumor Xenografts

Samantha Y.A. Terry[1], Keelara Abiraj[2], Cathelijne Frielink[1], Laura K. van Dijk[1,3], Johan Bussink[3], Wim J. Oyen[1], and Otto C. Boerman[1]

*[1]Department of Nuclear Medicine, Radboud UMC, Nijmegen, The Netherlands; [2]F. Hoffmann-La Roche AG, Pharma Research & Early Development, Basel, Switzerland; and [3]Department of Radiation Oncology, Radboud UMC, Nijmegen, The Netherlands*

Arginine-glycine-aspartic acid (RGD)–based imaging tracers allow specific imaging of integrin $\alpha_v\beta_3$, a protein overexpressed during angiogenesis, leading to the possibility that it might serve as a tool to stratify patients for antiangiogenic treatment. However, these tracers have generally been characterized in xenograft models in which integrin $\alpha_v\beta_3$ was constitutively expressed by the tumor cells themselves. In the studies presented here, the use of $^{111}$In-RGD$_2$ as a tracer to image only integrin $\alpha_v\beta_3$ expression on blood vessels in the tumor was determined using tumor xenografts in which tumor cells were integrin $\alpha_v\beta_3$-negative. **Methods:** DOTA-E-[c(RGDfK)]$_2$ was radiolabeled with $^{111}$In ($^{111}$In-RGD$_2$), and biodistribution studies were performed in squamous cell carcinoma of the head and neck (HNSCC) xenograft mouse models to determine the optimal peptide dose to image angiogenesis. Next, biodistribution and imaging studies were performed at the optimal peptide dose in 3 HNSCC mouse models, FaDu, SCCNij3, and SCCNij202. Immunohistochemical analysis of tumor vascular and cell surface expression of integrin $\alpha_v\beta_3$ and correlation analysis of vascular integrin $\alpha_v\beta_3$ and autoradiography were completed. **Results:** All 3 HNSCC xenografts expressed integrin $\alpha_v\beta_3$ on the vessels only. The optimal peptide dose of $^{111}$In-RGD$_2$ was 1 μg or less for specific integrin $\alpha_v\beta_3$–mediated uptake of the tracer. SPECT/CT imaging showed clear uptake of the tracer in the periphery of the tumors, corresponding with well-vascularized areas of the tumor. Within the tumor, $^{111}$In-RGD$_2$ autoradiography coincided with vascular integrin $\alpha_v\beta_3$ expression, as determined immunohistochemically. Integrin $\alpha_v\beta_3$–mediated uptake was also detected in nontumor tissues, which, through immunohistochemical analysis, proved positive for integrin $\alpha_v\beta_3$. **Conclusion:** $^{111}$In-RGD$_2$ allows the visualization of integrin $\alpha_v\beta_3$ in xenograft models in which integrin $\alpha_v\beta_3$ is expressed only on the neovasculature, such as in the HNSCC tumors. Thus, $^{111}$In-RGD$_2$ allows specific visualization of angiogenesis in tumor models lacking constitutive tumoral integrin $\alpha_v\beta_3$ expression but may be less useful for this purpose in many tumors in which tumor cells express integrin $\alpha_v\beta_3$.

**Key Words:** integrin $\alpha_v\beta_3$; dimeric RGD; head and neck carcinoma; SPECT imaging; angiogenesis

**J Nucl Med 2014; 55:281–286**
DOI: 10.2967/jnumed.113.129668

Angiogenesis, one of the hallmarks of cancer (*1*), refers to the formation of new blood vessels from preexisting vessels. It is initiated to increase nutrient and oxygen accessibility to tumor cells located far from the original vessels and includes the stabilization of hypoxia-inducible factor HIF-1α. Also, cytokines and growth factors, such as vascular endothelial growth factor (VEGF-A), are released into the microenvironment (*2–4*). Early during angiogenesis, endothelial cells become activated and express integrin $\alpha_v\beta_3$ (*2*). This receptor is crucial for the interaction of endothelial cells with extracellular matrix proteins, such as fibronectin or vitronectin, which occurs through their arginine-glycine-aspartic acid (RGD) tripeptide sequence (*5*). Angiogenesis-induced integrin expression on endothelial cells is related to cell survival and migration. However, integrins can also be expressed on the tumor cell surface and can thereby influence the invasion and movement of tumor cells across the vessels (*6*).

A cyclic peptide based on the RGD sequence, cilengitide, has been developed that shows promising results in the treatment of glioblastomas and other tumor types (*7*). Increased applications of other antiangiogenic therapies, such as the anti-VEGF antibody bevacizumab and small-molecule tyrosine kinase inhibitors, including sorafenib and sunitinib (*8*), have triggered an interest in nuclear imaging of angiogenesis. One way antiangiogenic therapy response can be measured is with dynamic contrast-enhanced MR imaging (*9*); however, this technique evaluates angiogenesis indirectly by measuring blood volume and permeability and many factors including biomarker validation and qualification hinder a wide application of dynamic contrast-enhanced MR imaging techniques in clinical trials. Imaging methods using radiolabeled RGD peptides could provide more specific and earlier feedback on the effect of antiangiogenic therapy on angiogenesis.

These tracers have the potential to select patients who might benefit from treatment with antiangiogenic drugs, beyond short-term tumor control. It is especially important to be able to monitor the efficacy of these therapies early on, considering overall survival is prolonged in only a limited group of patients, yet most patients encounter side effects such as hand-foot syndrome. Being able to image a response to antiangiogenic therapy using RGD-based tracers is of even greater importance when considering that standard methods of measuring tumor response according to Response Evaluation Criteria in Solid Tumors do not suffice when monitoring antiangiogenic therapy (*10*).

Previously, several avenues have been explored to develop angiogenic imaging tracers. These include radiolabeled VEGF isoforms, antibodies against VEGF, and RGD-based peptides against

Received Jul. 23, 2013; revision accepted Oct. 10, 2013.
For correspondence or reprints contact: Samantha Terry, Department of Nuclear Medicine, Radboud UMC, P.O. Box 9101, 6500 HB Nijmegen, The Netherlands.
E-mail: samantha.terry@radboudumc.nl
Published online Jan. 9, 2014.

integrin $\alpha_v\beta_3$ (*11*). RGD-based tracers have a major advantage because of their hydrophilicity and low molecular weight, enabling fast clearance via the kidneys while retaining high tumor uptake. These tracers might therefore enable early monitoring of antiangiogenic therapy (*12,13*).

It was previously determined that cyclic, multimeric RGD-based peptides display a higher target binding affinity than linear, monomeric variants (*14,15*). Radiolabeled peptides proved a good tracer for imaging tumors expressing integrin $\alpha_v\beta_3$ by either PET or SPECT and for imaging non–tumor-associated angiogenesis (*16*). The efficacy of using these peptides was determined with ovarian, renal cell carcinoma, and glioblastoma preclinical models (*12,15, 17–19*); however, these models are not ideal to determine whether RGD-based tracers allow the imaging of angiogenesis because tumoral expression of integrin $\alpha_v\beta_3$ was not excluded. In general, therefore, because of the constitutive integrin $\alpha_v\beta_3$ on tumor cells, these models do not allow the effects of constitutive integrin $\alpha_v\beta_3$ expression to be isolated from vascular integrin expression. Other RGD-based tracers have also been characterized in preclinical models in which integrin $\alpha_v\beta_3$ is expressed on the surface of tumor cells (*20*).

Here, we provide evidence that RGD-based tracers can image angiogenesis. $^{111}$In-$RGD_2$ was used in in vivo head and neck squamous cell carcinoma (SCC) xenografts in which integrin $\alpha_v\beta_3$ was expressed on angiogenesis-induced vessels only.

## MATERIALS AND METHODS

### Radiolabeling

For labeling with $^{111}$In, DOTA-E-[c(RGDfK)]$_2$ ($RGD_2$; Peptides International) was dissolved in 0.1 M 2-(*N*-morpholino)ethanesulfonic acid, pH 5.5, with 3 mM gentisic acid (Sigma-Aldrich). Subsequently, 1–90 MBq of $^{111}InCl_3$ (Covidien) per microgram of peptide was added. After 20 min at 95°C, the radiochemical purity was determined using instant thin-layer chromatography on silica gel strips (Gelman Sciences, Inc.) with 0.15 M sodium citrate buffer, pH 5.5, as the mobile phase.

Quality control was also performed using reversed-phase high-performance liquid chromatography on a C-18 Agilent Eclipse column (4.6 × 150 mm; Phenomenex). The column was eluted at a flow rate of 1 mL/min with a gradient of 97% buffer A at 0–5 min and 80% buffer A to 75% buffer A at 5–25 min (buffer A, 0.1% v/v trifluoroacetic acid in $H_2O$; buffer B, 0.1% v/v trifluoroacetic acid in acetonitrile). The preparations were analyzed on an Agilent 1200 system (Agilent Technologies). Radioactivity was monitored using an in-line NaI radiodetector (Raytest GmbH), and elution profiles were analyzed using Gina-star software (Raytest GmbH).

When radiochemical purity was less than 95%, radiolabeled $RGD_2$ was purified by an Oasis HLB 1-mL (10 mg) cartridge in 50% ethanol. Before being used in vivo, the ethanol was evaporated at 95°C and the peptide was diluted with 0.5% bovine serum/phosphate-buffered saline.

### In Vivo Tumor Models

FaDu human pharynx SCC cells were cultured in RPMI-1640 medium supplemented with 10% (v/v) fetal calf serum and 1% glutamine (Invitrogen). Cells were maintained at 37°C in a humidified 5% $CO_2$ atmosphere and routinely passaged using a 0.25% trypsin/ethylenediaminetetraacetic acid solution (Invitrogen). Patient-derived SSCNij202 and SSCNij3 head and neck SCC (HNSCC) xenografts were maintained in female BALB/c *nu/nu* mice (*21,22*). In the right flank of 6- to 8-wk-old female nude BALB/c *nu/nu* mice (Janvier), $5 \times 10^6$ FaDu cells in 200 μL of medium were injected subcutaneously, or a 1 $mm^3$ viable piece of SCCNij202 or SCCNij3 tumor xenografts was transplanted under anesthesia.

Experiments were performed 2 wk after inoculation for the FaDu model and 6 wk for both SCCNij models when tumors reached a volume of approximately 200 $mm^3$ as measured by caliper. All animal experiments were approved by the local Animal Welfare Committee in accordance with Dutch legislation and performed in accordance to their guidelines. The institutional review board approved this study in mice with human tumor xenografts.

### Biodistribution Studies

In biodistribution studies, to determine the optimal tumor model for the dose-finding studies, mice with FaDu, SCCNij3, or SCCNij202 xenografts were injected intravenously with 0.1 μg of $^{111}$In-$RGD_2$ (<1 MBq) plus ($n = 3$) or without ($n = 2$) 50 μg of cold, unlabeled peptide in 200 μL of 0.5% bovine serum albumin/phosphate-buffered saline. Mice were euthanized by $CO_2/O_2$ asphyxiation 1 h after injection. Blood, tumor, and major organs and tissues were dissected, weighed, and counted in a γ counter. The percentage injected dose per gram (%ID/g) was determined for each sample.

In dose-finding studies, mice with FaDu xenografts were injected with 0.01–100 μg of $^{111}$In-$RGD_2$ (<1 MBq), and biodistribution data were collected at 1 h after injection ($n = 5$) as before.

Biodistribution studies were then performed in all 3 HNSCC models (FaDu, SCCNij3, and SCCNij202) at 1 h after injection of 1 μg of $^{111}$In-$RGD_2$ (<1 MBq; $n = 3$). The receptor-mediated localization of the radiolabeled peptide was investigated by determining the biodistribution of $^{111}$In-$RGD_2$ in the presence of an excess (50-fold) of unlabeled peptide ($n = 2$).

### Immunohistochemistry

Antibodies against human integrin $\alpha_v\beta_3$ (LM609; MAB19976B [Millipore]), murine integrin $\beta_3$ (CD61; 550541 [BD PharMingen]), and murine vasculature (9F1; Department of Pathology at RUNMC) were used to determine expression of the respective antigens on 5-μm flash-frozen tumor or tissue sections. Briefly, sections were fixed in acetone and incubated with primary antibody, followed with a secondary biotinylated (CD61) or peroxidase-conjugated (9F1) antibody or with a primary, directly biotinylated, antibody (LM609). Tumor sections stained for CD61 and LM609 were then exposed to an avidin–biotin–enzyme complex (Vector Laboratories). Finally, tumor sections were incubated with diaminobenzidine for development (LM609, CD61, 9F1), followed by a hematoxylin counterstain. Adjacent tumor sections were also stained with hematoxylin and eosin.

### Correlation Analysis of Autoradiography and CD61 Staining

Flash-frozen tumor sections (10 μm) from mice injected intravenously with $^{111}$In-$RGD_2$ (14–25 MBq) were exposed to a phosphor imaging screen overnight, which was scanned in a phosphor imager system (Bioimaging Analyzer System 1800-II; Fujifilm) at a pixel size of 50 × 50 μm.

The immunohistochemistry of adjacent sections and autoradiography gray-value images (gray scale range, 0–255) were overlaid using Photoshop (CS4, version 11.0.2; Adobe). The pixel and figure size of the autoradiographic image was bicubically rescaled to the immunohistochemistry image for alignment (50 × 50 μm). Subsequently, images were upscaled (250 × 250 μm) to compensate for image coregistration errors and scattering of the tracer signal. After alignment, regions of interest drawn previously for excluding necrosis in immunohistochemical analysis were masked in the autoradiography image. Coregistered pixel gray values were determined with ImageJ (version 1.43m, JAVA-based image-processing package National Institutes of Health) using the JACoP plugin package. Only pixels containing viable tumor tissue were included in the pixel-by-pixel Spearman correlation analysis.

### Micro-SPECT/CT

In micro-SPECT imaging studies, mice with FaDu, SCCNij3, or SCCNij202 tumor xenografts were injected intravenously with 1 μg of

$^{111}$In-RGD$_2$ (14–25 MBq). A 50-fold cold excess of RGD$_2$ was coinjected to investigate receptor-mediated localization of the radiolabeled peptide. One hour after injection, mice were euthanized by $CO_2/O_2$ asphyxiation and scanned on their flank using the U-SPECT-II/CT (MILabs) (*23*). Mice were euthanized before imaging, rather than imaged under anesthesia, to exclude movement artifacts and to allow direct comparison of the SPECT/CT images with the biodistribution data. Static SPECT scans were acquired as 3 frames of 20 min, followed by a CT scan for anatomic reference (SPECT: spatial resolution 160 μm, 65 kV, 615 μA). SPECT/CT scans, all 3 frames combined, were reconstructed with software from MILabs, using an ordered-subset expectation maximization algorithm, with a voxel size of 0.4 mm.

### Statistical Analysis

In biodistribution studies, all mean values are given as ±SD. Statistical analysis in biodistribution studies was performed using a 1-sample *t* test with GraphPad Prism (version 5.03; GraphPad Software).

## RESULTS

### Radiolabeling

A maximum specific activity of 75 MBq of $^{111}$In-RGD$_2$ per microgram was obtained. At these high specific activities, purification was effective, and a radiochemical purity of greater than 95% could be achieved (Fig. 1).

### Biodistribution Studies

The specific uptake of 0.1 μg of $^{111}$In-RGD$_2$ was determined in each of the HNSCC models (Fig. 2). Tumor uptake of $^{111}$In-RGD$_2$ in the FaDu, SCCNij3, and SCCNij202 HNSCC models was 2.37 ± 0.53, 2.55 ± 0.29, and 2.8 ± 1.16 %ID/g, respectively. The highest specific uptake was seen for the FaDu model as the ratio of $^{111}$In-RGD$_2$ to $^{111}$In-RGD$_2$-plus-cold-excess, equal to 6, compared with a ratio equal to 4 found for both SCCNij3 and SCCNij202 tumor xenograft models.

The results of the protein dose–escalation study with $^{111}$In-RGD$_2$ in the mice with FaDu tumors are summarized in Figure 3. Tumor uptake of $^{111}$In-RGD$_2$ at 1 h after injection was maximal at doses of 1 μg of $^{111}$In-RGD$_2$ or less: 1.27 ± 0.52 and 1.37 ± 0.37 %ID/g at 0.01 and 1 μg, respectively ($P = 0.56$). $^{111}$In-RGD$_2$ uptake in nontumor tissues, such as the spleen and duodenum, decreased with increasing doses of $^{111}$In-RGD$_2$, indicating that tracer uptake is integrin $\alpha_v\beta_3$–mediated and saturated earlier than tracer uptake in the tumor. Injection of 1 μg of $^{111}$In-RGD$_2$ resulted in 1.26 ± 0.22 and 2.37 ± 0.40 %ID/g tracer uptake in the spleen and duodenum, respectively, significantly lower than the uptake of 0.01 μg of $^{111}$In-RGD$_2$ in these tissues, which was 2.14 ± 0.31 and 4.16 ± 1.11 %ID/g, respectively ($P = 0.0009$ and 0.0006, respectively). A dose of 1 μg of $^{111}$In-RGD$_2$ was therefore determined as optimal, showing the highest tumor uptake and the lowest uptake in nontumor tissues.

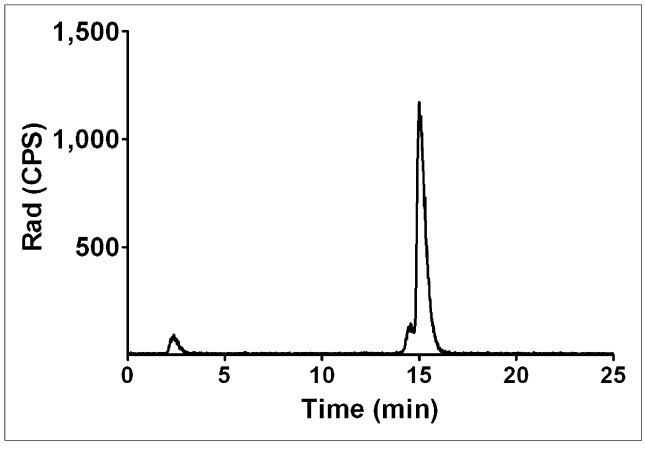


**FIGURE 1.** Postpurification reversed-phase high-performance liquid chromatogram showing greater than 95% radiochemical purity of $^{111}$In-RGD$_2$ and less than 5% $^{111}$In-ethylenediaminetetraacetic acid, each with elution time of 15 and 2 min, respectively.

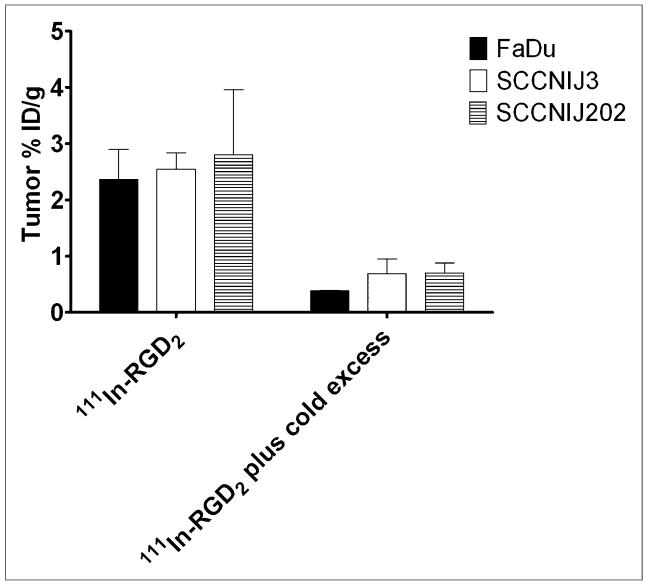


**FIGURE 2.** Biodistribution of 0.1 μg of $^{111}$In-RGD$_2$ at 1 h after injection in BALB/c nude mice with FaDu, SCCNij3, or SCCNij202 tumors in absence or presence of excess of nonradiolabeled RGD$_2$. Results are mean ± SD bars.

Tumor uptake of 1 μg of $^{111}$In-RGD$_2$ at 1 h after injection differed among the 3 HNSCC models used, as shown in Figure 4. Tumor uptake was 2.25 ± 0.02, 1.94 ± 0.54, and 1.21 ± 0.04 %ID/g for FaDu, SCCNij3, and SCCNij202, respectively. Tumor-to-blood ratios of $^{111}$In-RGD$_2$ averaged 12.3 and were not significantly different among the 3 HNSCC models (data not shown). Tumor uptake in the FaDu, SCCNij3, and SCCNij202 models is integrin $\alpha_v\beta_3$–mediated, because the addition of 50 μg of unlabeled RGD$_2$ decreased the uptake to 0.74 ± 0.41, 0.60 ± 0.00, and 0.49 ± 0.10 %ID/g, respectively (Fig. 4).

### Immunohistochemical Analysis

Through immunohistochemical analysis of murine integrin $\alpha_v\beta_3$, it was determined that nontumor tissues, including the lung, spleen, and duodenum, expressed integrin $\alpha_v\beta_3$ (Fig. 5). The immunohistochemical results for tumoral integrin $\alpha_v\beta_3$ (LM609) and integrin $\alpha_v\beta_3$ expression on murine vasculature (CD61) within all 3 HNSCC xenografts are summarized in Table 1. FaDu, SCCNij3, and SCCNij202 tumors were all negative for LM609 and positive, to varying degrees, for CD61. All vessels stained for CD61 were also positive for the general murine vasculature marker 9F1; however, not all 9F1-positive vessels stained for CD61 (data not shown). This is in line with the hypothesis that integrin $\alpha_v\beta_3$, as measured by CD61, is expressed only on newly formed blood vessels in these tumors.

### Correlation of Vascular Integrin $\alpha_v\beta_3$ and Autoradiography

Correlation analysis of vascular integrin $\alpha_v\beta_3$ expression, as determined by CD61 immunohistochemistry, and localization of $^{111}$In-RGD$_2$, deduced by autoradiography, confirmed specific targeting of

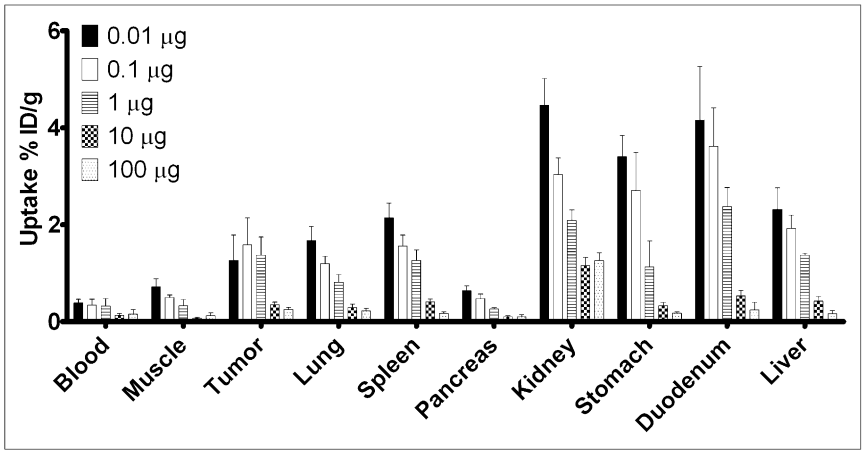


**FIGURE 3.** Biodistribution of 0.01–100 μg of $^{111}$In-RGD$_2$ at 1 h after injection in BALB/c nude mice with FaDu tumors. Results are mean ± SD bars.

the tracer for vascular integrin $\alpha_v\beta_3$, with a Spearman r value of 0.76 ($P < 0.0001$; Fig. 6).

### SPECT/CT Imaging

Fused SPECT/CT scans (Fig. 7) show images that were in line with the biodistribution data. On these scans, FaDu and SCCNij202 tumors were clearly visualized with $^{111}$In-labeled RGD$_2$. The integrin $\alpha_v\beta_3$ specificity of $^{111}$In-RGD$_2$ in vivo was demonstrated in a blocking experiment in which the tracer was coinjected with an excess of nonradiolabeled RGD$_2$, resulting in decreased tumor accumulation of the tracer, compared with radiolabeled RGD$_2$ alone (Fig. 7). Tumor uptake of $^{111}$In-RGD$_2$ was mostly localized to the periphery of the tumor.

## DISCUSSION

In this study, HNSCC tumor models were used in which integrin $\alpha_v\beta_3$ expression was solely expressed on the tumor vasculature,

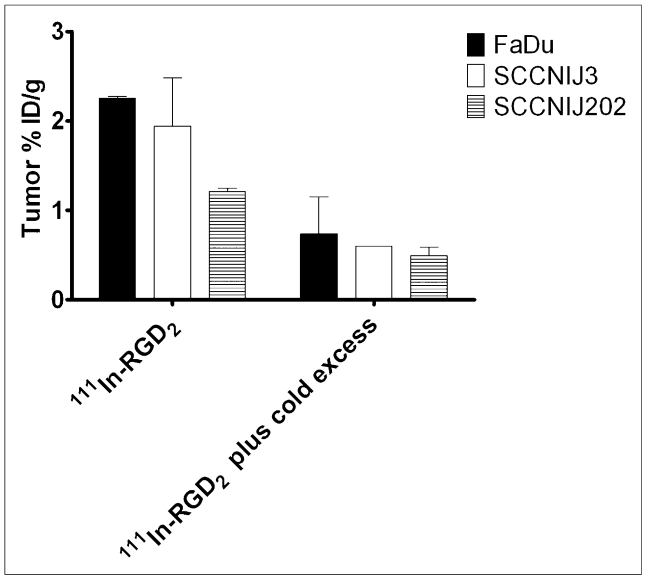


**FIGURE 4.** Tumoral uptake of 1 μg of $^{111}$In-RGD$_2$ at 1 h after injection in BALB/c nude mice with FaDu, SCCNij3, or SCCNij202 tumors in absence or presence of excess of nonradiolabeled RGD$_2$. Results are mean ± SD bars.

making these models ideal to investigate the potential of tracers, such as $^{111}$In-RGD$_2$, to image angiogenesis. Initially, 13 HNSCC patient–derived tumor xenograft models were stained for integrin $\alpha_v\beta_3$, and 12 of 13 were negative for constitutive tumoral expression of integrin $\alpha_v\beta_3$. Ten of 13 HNSCC xenografts were positive to varying degrees for angiogenesis-induced integrin $\alpha_v\beta_3$ expression (data not shown), confirming the previous findings of Beer et al. (*24*). Of these 13 xenograft tumor models, SCCNij3 and SCCNij202 were chosen, alongside the cell culture–derived FaDu tumor model, for the experiments presented here.

The results reported here describe how these tumors models have enabled us to verify the potential of $^{111}$In-RGD$_2$ as a specific antiangiogenic marker in HNSCC, a feature that, despite much clinical and preclinical research into radiolabeled RGD peptides as a tracer for integrin $\alpha_v\beta_3$ (*11,18,20,25,26*), was still uncertain. SPECT/CT imaging showed clear uptake of the tracer in areas corresponding with vascularized areas of the tumor. Correlation analysis allowed us to further determine areas within the tumor in which $^{111}$In-RGD$_2$ was located, as determined by autoradiography, and coincided with vascular integrin $\alpha_v\beta_3$ expression, as measured after immunohistochemical staining.

There has been some indication from the literature that RGD-based tracers can target integrin $\alpha_v\beta_3$ expressed on tumor vessels. For instance, the uptake of $^{18}$F-AH111585 in LLC and Calu-6 lung carcinoma models was attributed solely to integrin $\alpha_v\beta_3$ expression on murine vasculature (*27*); however, it was assumed that these tumors did not constitutively express integrin $\alpha_v\beta_3$ based only on in vitro binding studies using $^{99m}$Tc-d-c(RGDfK) (*28*). Here, biodistribution studies using 3 HNSCC models provide the first concrete evidence that $^{111}$In-RGD$_2$ can be used as an angiogenesis-specific imaging tracer. The tracer accumulated in tumors that did not constitutively express integrin $\alpha_v\beta_3$, and this accumulation was target-specific because coinjection with an excess of unlabeled peptide decreased tumor uptake of $^{111}$In-RGD$_2$. Interestingly, the amount of $^{111}$In-RGD$_2$ uptake within the FaDu, SCCNij3, and SCCNij202 tumor xenografts did not correspond with the varying degrees of vascular integrin $\alpha_v\beta_3$ expression described in Table 1. A correlation between integrin expression and tumor accumulation of $^{18}$F-galacto-RGD was, however, observed in imaging studies using melanoma tumor models, in which integrin-positive and -negative tumors were injected at varying ratios (*29*). The lack of correlation between the uptake of the RGD$_2$ tracer in the HNSCC tumors and integrin $\alpha_v\beta_3$ expression levels is most likely due to a combination of integrin $\alpha_v\beta_3$ expression levels and the anatomy of the tumor, because the percentage necrosis varied considerably between the models, which could affect tracer uptake levels.

Comparison of the uptake of $^{111}$In-RGD$_2$ in the HNSCC tumors described here with the tumor uptake in NIH:OVCAR-3 xenografts also suggests that the present experiments provide evidence that $^{111}$In-RGD$_2$ can be used to visualize angiogenesis specifically. Janssen et al. showed that the average uptake of 0.5 μg of $^{111}$In-RGD$_2$ ranged between 6 and 8 %ID/g and that tumor uptake did not change between 30 min and 8 h after injection of the tracer (*18*). A similar tumor uptake of 6 %ID/g was seen in the renal cell carcinoma SK-RC-52 model, in which, as in the ovarian carcinoma

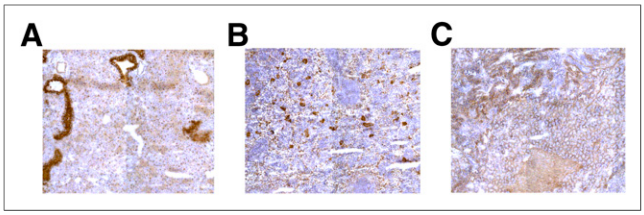


**FIGURE 5.** Immunohistochemical staining for murine integrin $\alpha_v\beta_3$ on frozen 5-μm sections of lung (A), spleen (B), and duodenum (C) of BALB/c nude mouse. Magnification equals ×20.

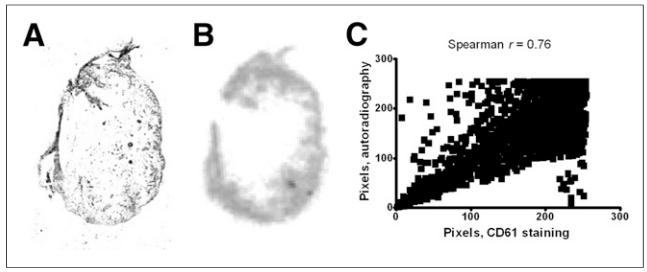


**FIGURE 6.** CD61 immunohistochemistry (A) and autoradiography (B) and correlation analysis (C) of 5- and 10-μm SCCNij202 tumor xenografts, respectively.

tumors, integrin $\alpha_v\beta_3$ is also expressed constitutively on the tumor cells (*15,19*). Uptake of other radiolabeled dimeric RGD tracers also averaged around 5–10 %ID/g in the SK-RC-52, OVCAR-3, and glioma tumor models (*17,30–33*). The average uptake of $^{111}$In-RGD$_2$ in the HNSCC tumors approximates 1.3 %ID/g, suggesting that only vascular integrin $\alpha_v\beta_3$ expression has any influence on the tumor uptake of $^{111}$In-RGD$_2$ and that therefore total tumor uptake is lower than in tumor models in which integrin $\alpha_v\beta_3$ is expressed constitutively. Uptake of radiolabeled DOTA-RGD$_2$ at 1 h after injection in integrin-negative melanoma xenografts (*34*) was approximately the same as in the integrin-negative HNSCC tumors, suggesting that in all tumors in which integrin $\alpha_v\beta_3$ is not expressed constitutively, uptake of the tracer will be approximately 1 %ID/g and can be ascribed to neovascularity. However, the M21L integrin–negative tumors were derived from parental integrin-expressing melanoma cells in vitro, making the HNSCC models used here more representative of the clinic because 10 of 13 patient-derived HNSCC tumor sections were positive only for integrin $\alpha_v\beta_3$ on the vessels.

The tumor uptake of dimeric RGD imaging peptides previously correlated well with integrin $\alpha_v\beta_3$ expression on the vasculature of otherwise integrin $\alpha_v\beta_3$–negative colorectal tumor xenografts (*35*). However, in patients with colorectal cancer, this imaging tracer would not be a specific angiogenesis imaging tool, because unlike the area of the head and neck, the gastrointestinal system constitutively expresses integrin $\alpha_v\beta_3$, even in the absence of tumor-associated angiogenesis.

Integrin expression within nontumor tissues, such as the lung, spleen, and intestine, hampers the identification of lesions within or near these areas. The development of multimeric RGD peptides to enhance specific uptake in integrin $\alpha_v\beta_3$–expressing tumors through multidentate binding sites (*36–38*) was thought to reduce specific uptake in nontumor tissues. Despite the multimeric nature of $^{111}$In-RGD$_2$, uptake of the tracer was still visualized in these nontumor tissues, as seen in the biodistribution studies described here. The issues with lesion identification therefore still stand, however, as Figure 3 suggests, the nontumor targeting of $^{111}$In-RGD$_2$ can most likely be reduced by determining the optimal peptide dose.

**TABLE 1**
Integrin $\alpha_v\beta_3$ Expression on Tumor Cells (LM609) and New Blood Vessels (CD61) of HNSCC Subcutaneous Tumor Xenografts

| Tumor model | LM609 | CD61 |
|---|---|---|
| FaDu | — | +/++ |
| SCCNij3 | — | ++ |
| SCCNij202 | — | ++/+++ |

On the basis of the data presented here, $^{111}$In-RGD$_2$ does allow the specific visualization of angiogenesis in tumor models lacking constitutive tumoral integrin $\alpha_v\beta_3$ expression, such as HNSCC. Although clinically speaking, a lack of integrin $\alpha_v\beta_3$ expression on tumor cells is not a prerequisite for use in conjunction with antiangiogenic therapy, this will be required if the response to

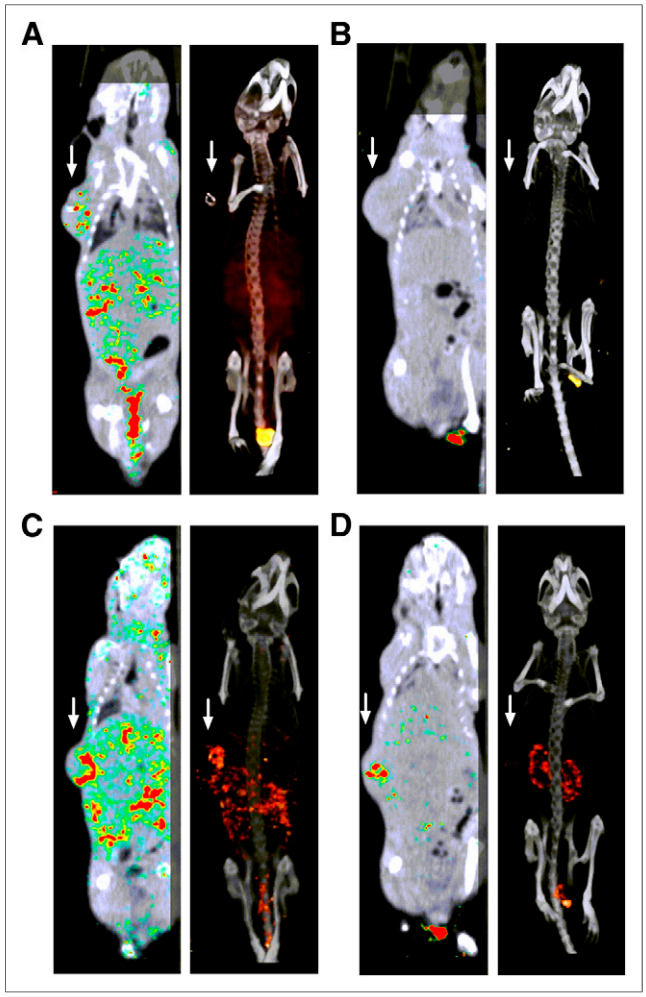


**FIGURE 7.** Anterior 2-dimensional (left) and 3-dimensional (right) volume projections of fused SPECT/CT scans of mice with subcutaneous FaDu (A and B) or SCCNij202 (C and D) tumor xenografts on right flank. Mice were injected with either $^{111}$In-RGD$_2$ (A and C) or with $^{111}$In-RGD$_2$ plus cold excess (B and D). Static scans were recorded at 1 h after injection. Arrows point to tumor location.

antiangiogenic therapy is solely based on RGD-based tracers or if patients will be stratified or monitored for antiangiogenic therapy or response using these tracers. The exact extent of integrin $\alpha_v\beta_3$ expression on various tumor types, however, is not yet known and will need to be further determined before this tracer is used as single marker for response to antiangiogenic therapy.

## CONCLUSION

$^{111}$In-RGD$_2$ allows the visualization of integrin $\alpha_v\beta_3$ in xenografts models in which integrin $\alpha_v\beta_3$ is expressed only on the neovasculature. It can therefore be stated that $^{111}$In-RGD$_2$ does allow the specific visualization of angiogenesis in tumor models lacking constitutive tumoral integrin $\alpha_v\beta_3$ expression, such as HNSCC. $^{111}$In-RGD$_2$ may therefore allow selection of patients who will benefit from treatment with antiangiogenic drugs, and may monitor the efficacy of these therapies early on.

## DISCLOSURE

The costs of publication of this article were defrayed in part by the payment of page charges. Therefore, and solely to indicate this fact, this article is hereby marked "advertisement" in accordance with 18 USC section 1734. This study was funded in part by the Roche Postdoc Fellowship (RPF) Program. No other potential conflict of interest relevant to this article was reported.

## ACKNOWLEDGMENTS

We thank Peter Zijderveld, Bianca Lemmers-van de Weem, Iris Lamers-Elemans, and Henk Arnts for technical assistance.

## REFERENCES

1. Hanahan D, Weinberg RA. Hallmarks of cancer: the next generation. *Cell.* 2011;144:646–674.
2. Weis SM, Cheresh DA. Tumor angiogenesis: molecular pathways and therapeutic targets. *Nat Med.* 2011;17:1359–1370.
3. Weis SM, Cheresh DA. αV integrins in angiogenesis and cancer. *Cold Spring Harb Perspect Med.* 2011;1:a006478.
4. Bergers G, Benjamin LE. Tumorigenesis and the angiogenic switch. *Nat Rev Cancer.* 2003;3:401–410.
5. Ruoslahti E, Pierschbacher MD. New perspectives in cell adhesion: RGD and integrins. *Science.* 1987;238:491–497.
6. Brakebusch C, Bouvard D, Stanchi F, Sakai T, Fassler R. Integrins in invasive growth. *J Clin Invest.* 2002;109:999–1006.
7. Mas-Moruno C, Rechenmacher F, Kessler H. Cilengitide: the first anti-angiogenic small molecule drug candidate design, synthesis and clinical evaluation. *Anticancer Agents Med Chem.* 2010;10:753–768.
8. Samant RS, Shevde LA. Recent advances in anti-angiogenic therapy of cancer. *Oncotarget.* 2011;2:122–134.
9. O'Connor JP, Jackson A, Parker GJ, Roberts C, Jayson GC. Dynamic contrast-enhanced MRI in clinical trials of antivascular therapies. *Nat Rev Clin Oncol.* 2012;9:167–177.
10. Desar IM, van Herpen CM, van Laarhoven HW, Barentsz JO, Oyen WJ, van der Graaf WT. Beyond RECIST: molecular and functional imaging techniques for evaluation of response to targeted therapy. *Cancer Treat Rev.* 2009;35:309–321.
11. Dijkgraaf I, Boerman OC. Radionuclide imaging of tumor angiogenesis. *Cancer Biother Radiopharm.* 2009;24:637–647.
12. Wu H, Chen H, Sun Y, et al. Imaging integrin $\alpha_v\beta_3$ positive glioma with a novel RGD dimer probe and the impact of antiangiogenic agent (Endostar) on its tumor uptake. *Cancer Lett.* 2013;335:75–80.
13. Battle MR, Goggi JL, Allen L, Barnett J, Morrison MS. Monitoring tumor response to antiangiogenic sunitinib therapy with $^{18}$F-fluciclatide, an $^{18}$F-labeled $\alpha_v\beta_3$-integrin and $\alpha_v\beta_5$-integrin imaging agent. *J Nucl Med.* 2011;52:424–430.
14. Gurrath M, Muller G, Kessler H, Aumailley M, Timpl R. Conformation/activity studies of rationally designed potent anti-adhesive RGD peptides. *Eur J Biochem.* 1992;210:911–921.
15. Dijkgraaf I, Kruijtzer JA, Liu S, et al. Improved targeting of the $\alpha_v\beta_3$ integrin by multimerisation of RGD peptides. *Eur J Nucl Med Mol Imaging.* 2007;34:267–273.
16. Dimastromatteo J, Riou LM, Ahmadi M, et al. In vivo molecular imaging of myocardial angiogenesis using the $\alpha_v\beta_3$ integrin-targeted tracer $^{99m}$Tc-RAFT-RGD. *J Nucl Cardiol.* 2010;17:435–443.
17. Dijkgraaf I, Terry SYA, McBride WJ, et al. Imaging integrin α-v-β-3 expression in tumors with an $^{18}$F-labeled dimeric RGD peptide. *Contrast Media Mol Imaging.* 2013;8:238–245.
18. Janssen ML, Oyen WJ, Dijkgraaf I, et al. Tumor targeting with radiolabeled $\alpha_v\beta_3$ integrin binding peptides in a nude mouse model. *Cancer Res.* 2002;62:6146–6151.
19. Dijkgraaf I, Yim CB, Franssen GM, et al. PET imaging of $\alpha_v\beta_3$ integrin expression in tumours with $^{68}$Ga-labelled mono-, di- and tetrameric RGD peptides. *Eur J Nucl Med Mol Imaging.* 2011;38:128–137.
20. Haubner R, Wester HJ, Weber WA, et al. Noninvasive imaging of $\alpha_v\beta_3$ integrin expression using $^{18}$F-labeled RGD-containing glycopeptide and positron emission tomography. *Cancer Res.* 2001;61:1781–1785.
21. Ljungkvist AS, Bussink J, Kaanders JH, et al. Hypoxic cell turnover in different solid tumor lines. *Int J Radiat Oncol Biol Phys.* 2005;62:1157–1168.
22. Stegeman H, Kaanders JH, van der Kogel AJ, et al. Predictive value of hypoxia, proliferation and tyrosine kinase receptors for EGFR-inhibition and radiotherapy sensitivity in head and neck cancer models. *Radiother Oncol.* 2013;106:383–389.
23. van der Have F, Vastenhouw B, Ramakers RM, et al. U-SPECT-II: an ultra-high-resolution device for molecular small-animal imaging. *J Nucl Med.* 2009;50:599–605.
24. Beer AJ, Grosu AL, Carlsen J, et al. [$^{18}$F]galacto-RGD positron emission tomography for imaging of $\alpha_v\beta_3$ expression on the neovasculature in patients with squamous cell carcinoma of the head and neck. *Clin Cancer Res.* 2007;13:6610–6616.
25. Sivolapenko GB, Skarlos D, Pectasides D, et al. Imaging of metastatic melanoma utilising a technetium-99m labelled RGD-containing synthetic peptide. *Eur J Nucl Med.* 1998;25:1383–1389.
26. Beer AJ, Haubner R, Goebel M, et al. Biodistribution and pharmacokinetics of the $\alpha_v\beta_3$-selective tracer $^{18}$F-galacto-RGD in cancer patients. *J Nucl Med.* 2005;46:1333–1341.
27. Morrison MS, Ricketts SA, Barnett J, Cuthbertson A, Tessier J, Wedge SR. Use of a novel Arg-Gly-Asp radioligand, $^{18}$F-AH111585, to determine changes in tumor vascularity after antitumor therapy. *J Nucl Med.* 2009;50:116–122.
28. Jung KH, Lee KH, Paik JY, et al. Favorable biokinetic and tumor-targeting properties of $^{99m}$Tc-labeled glucosamino RGD and effect of paclitaxel therapy. *J Nucl Med.* 2006;47:2000–2007.
29. Haubner R, Weber WA, Beer AJ, et al. Noninvasive visualization of the activated $\alpha_v\beta_3$ integrin in cancer patients by positron emission tomography and [$^{18}$F]Galacto-RGD. *PLoS Med.* 2005;2:e70.
30. Dijkgraaf I, Liu S, Kruijtzer JA, et al. Effects of linker variation on the in vitro and in vivo characteristics of an $^{111}$In-labeled RGD peptide. *Nucl Med Biol.* 2007;34:29–35.
31. Janssen M, Oyen WJ, Massuger LF, et al. Comparison of a monomeric and dimeric radiolabeled RGD-peptide for tumor targeting. *Cancer Biother Radiopharm.* 2002;17:641–646.
32. Wu Z, Li ZB, Cai W, et al. $^{18}$F-labeled mini-PEG spacered RGD dimer ($^{18}$F-FPRGD2): synthesis and microPET imaging of $\alpha_v\beta_3$ integrin expression. *Eur J Nucl Med Mol Imaging.* 2007;34:1823–1831.
33. Shi J, Wang L, Kim YS, et al. 99mTcO(MAG2-3G3-dimer): a new integrin $\alpha_v\beta_3$-targeted SPECT radiotracer with high tumor uptake and favorable pharmacokinetics. *Eur J Nucl Med Mol Imaging.* 2009;36:1874–1884.
34. Decristoforo C, Hernandez Gonzalez I, Carlsen J, et al. $^{68}$Ga- and $^{111}$In-labelled DOTA-RGD peptides for imaging of $\alpha_v\beta_3$ integrin expression. *Eur J Nucl Med Mol Imaging.* 2008;35:1507–1515.
35. Liu Z, Jia B, Shi J, et al. Tumor uptake of the RGD dimeric probe $^{99m}$Tc-G(3)-2P(4)-RGD2 is correlated with integrin $\alpha_v\beta_3$ expressed on both tumor cells and neovasculature. *Bioconjug Chem.* February 25, 2010 [Epub ahead of print].
36. Shi J, Wang L, Kim YS, et al. Improving tumor uptake and excretion kinetics of $^{99m}$Tc-labeled cyclic arginine-glycine-aspartic (RGD) dimers with triglycine linkers. *J Med Chem.* 2008;51:7980–7990.
37. Wang L, Shi J, Kim YS, et al. Improving tumor-targeting capability and pharmacokinetics of $^{99m}$Tc-labeled cyclic RGD dimers with PEG(4) linkers. *Mol Pharm.* 2009;6:231–245.
38. Sancey L, Ardisson V, Riou LM, et al. In vivo imaging of tumour angiogenesis in mice with the $\alpha_v\beta_3$ integrin-targeted tracer $^{99m}$Tc-RAFT-RGD. *Eur J Nucl Med Mol Imaging.* 2007;34:2037–2047.